Synthesis, FTIR, NMR, UV-Vis and Electrochemistry Analysis of Ferrocenyl Schiff Bases

Olatunde S. Oladeji[1, 2], Monisola I. Ikhile[1], Olusesan Ojo[1], Carine M. D. Fotsing[1], Messai Mamo[1], Patrick G. Ndungu[1,3], Derek T. Ndinteh[1].

[1]Department of Chemical Sciences, Faculty of Science, Doornfontein Campus, PMB 2028, University of Johannesburg, South Africa.

[2]Department of Chemical Sciences, Faculty of Natural Sciences, Ajayi Crowther University, PMB: 1066, Oyo Campus, Nigeria.

[3]Department of Chemistry, Faculty of Natural and Agricultural Science, University of Pretoria, Pretoria, 0001 Hatfield, South Africa.

[*] **Corresponding authors**:

E-mail addresses: dndinteh@uj.ac.za, (D. Ndinteh), os.oladeji@acu.edu.ng (O. Oladeji)

Abstract

Five derivatives of 3-ferrocenylphenylimine were synthesized through arylation of ferrocene by diazonium salt under phase transfer conditions. Sn/HCl was used to reduce the nitro derivatives to ferrocenylanilines, which was followed by addition of aromatic aldehydes. The thus obtained compounds N-(2,3-dimethoxybenzylidene)-3-ferrocenylimine (L_1), N-(4-nitrobenzylidene)-3-ferrocenylimine (L_4), N-(2-thiophenecarboxbenzylidene)-3-ferrocenylimine (L_5), N-(3-nitrobenzylidene)-3-ferrocenylimine (L_9), and N-(2-furabenzylidene)-3-ferrocenylimine (L_{10}) showed similar UV-vis absorption spectra with the exception of L_4 which is the nitro-substituted benzylideneimine. Cyclic voltammetry of peak potential separation of the compounds under light and dark conditions was studied and the redox couple ferrocene/ferrocenium showed half-wave potentials around 0.05 V vs. Ag/AgCl which is markedly higher than ferrocene. The dependence of the peak potentials and currents from the scan rates was studied in detail. While the energy of the highest occupied molecular orbital was obtained from the half-wave potential of the oxidation, the energy of the lowest unoccupied molecular orbital (LUMO) was estimated from the onset of the absorption spectra. The gaps range from 2.87 to 3.05 eV.

Graphical abstract

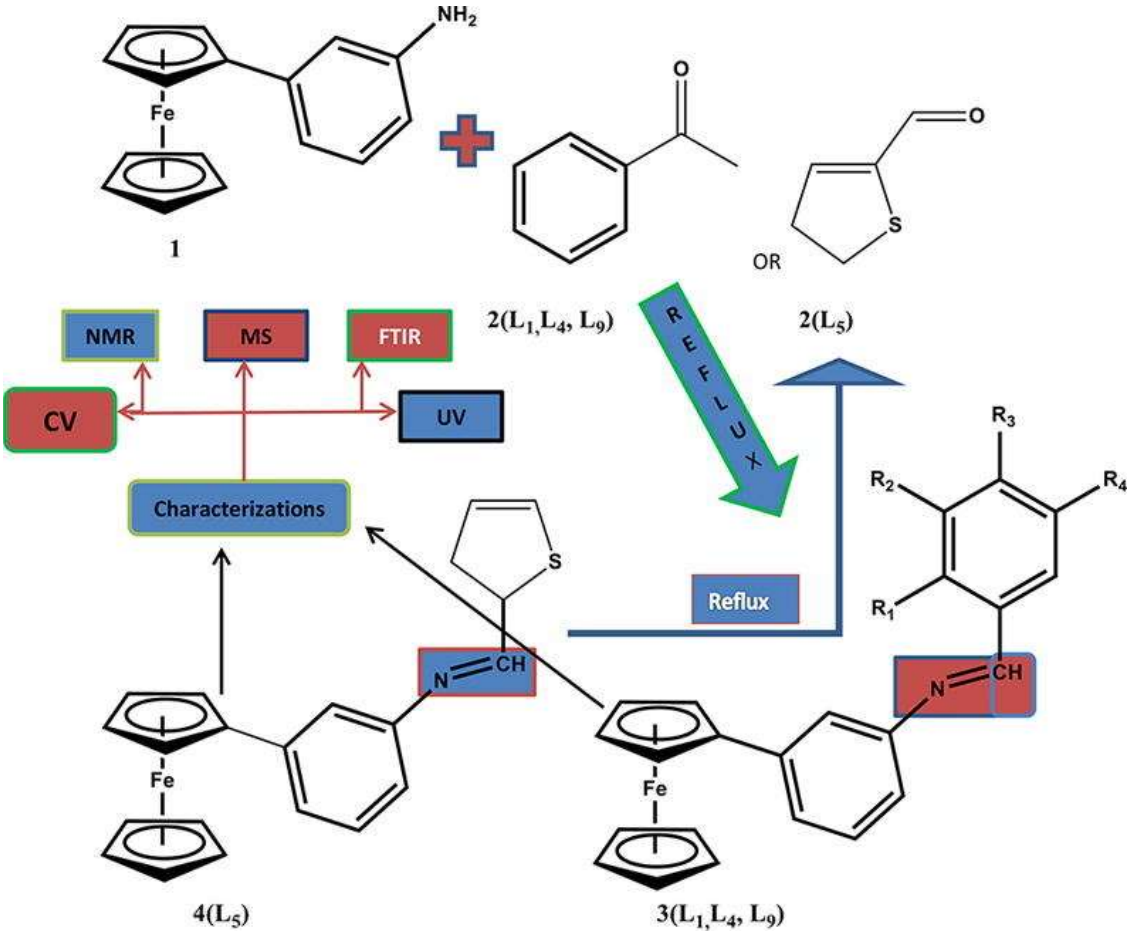

Keywords. Illumination, voltammograms, cyclopentadienyl, half-wave potential, voltammetry

Highlights

- Five novel compounds **L_1**, **L_4**, **L_5**, **L_9** and **L_{10}** were synthesized via arylation of ferrocene by diazonium salt under phase transfer condition.
- The cyclic voltammograms of compounds **L_1**, **L_4**, **L_5**, **L_9** and **L_{10}** showed a clear well-defined redox peak in both conditions .
- The calibration plots confirmed that **L_1**, **L_4**, **L_5**, **L_9**, and **L_{10}** showed reversible electron transfer processes and diffusion control processes.
- The LUMO energy levels give better electrons transportation compare to the LUMO energy level of the conduction band edge of TiO_2.

1. Introduction

Ferrocene body core was discovered over many decades ago by the serendipitous process in 1951. This revolution of ferrocene compounds has increased the growth of inorganic and bio-organometallic chemistry [1-7]. Cyclopentadienyl based compounds have shown number of applications as stoichiometric reagent in chemical research and precursor for metal hybrids and halides since its discovery which has been explored by many researchers. This is on the bases of its capability to easily functionalize cyclopentadienyl rings in ferrocene skeleton *via* electrophilic substitution, ability to easily undergo redox process, rigidity of the structure as a versatile in building block as well as its stability toward air, temperature and moisture has brought ferrocene to a limelight [8, 9]. However, in recent years, the electrochemistry of ferrocene compounds has displayed remarkable growth. The electrochemical properties among other ferrocenyl applications of various synthesized heterocyclic compounds has been well documented based on the presence of their heteroatoms and the reports have shown their outstanding performance in pharmaceutical, catalysis, sensor and energy generation molecular wire [10-20]. These performances are attributed to their capability to easily facilitate effective binding of oxygen reversibility [21, 22] their redox process [23, 24] and oxidative effect in DNA [25]. Ferrocenyl compounds have shown to be outstanding and robust building block based on its reversible 1e redox behaviour [26-29]. In line with this knowledge, some of ferrocenyl Schiff bases containing heteroatoms have been studied by various researchers to date in order to explore their effective redox properties in the various applications [30, 31]. The presence of azomethine (C=N) in ferrocenyl Schiff bases have found application in many areas. This includes electrochemical properties [44, 52, 53], biological activities such as tuberculosis [32], antibacterial [33-35], antifungal [36], antitumor [37], antiviral [37] and as active component in anticancer drug [38-40] as a result of imine linkage (CH=N-) present in the living systems [41]. This class of compounds are also find application in energy generation as dyes in Grätzel-type cells such as dye-sensitized solar cells [48, 50-51]. Despite numerous applications of ferrocenyl azomethine in several areas, the potential electrochemistry characterization of five 3-ferrocenylphenylimine are yet to be studied and there is need to effectively study them and the influence of their various substituents in order to provide a solution to current global electrochemistry challenges.

For this study, we reported synthesis, FTIR-, NMR-, UV-Vis and electrochemistry behaviour of five 3-ferrocenylphenylimine Schiff bases. They were synthesis via arylation of ferrocene by diazonium salt under phase transfer condition followed by refluxing with different aromatic aldehydes. The reduction of nitro derivatives was achieved via Sn/HCl [42].

2. Experimental

2.1. Materials and methods

For the synthesis of 3-ferrocenylphenylimine Schiff bases, all chemicals used were purchased from Sigma Aldrich and Protea laboratory solutions (Pty) Ltd, South Africa. Dry ethanol was used under nitrogen condition. Other chemicals were used without further purification. Bruker topspin ^{1}H NMR (500 MHz) and ^{13}C NMR (125 MHz) were used to elucidate the compounds. Fourier Transform Infrared FT-IR Spectra were recorded on a PerkinElmer (spectrum 100) FT-IR Spectrometer while ultra-violet visible (UV-Vis) spectrometry analysis was determined using Agilent Technologies Cary 60 UV-Vis. The melting points were carryout using Agilent 100 Melting point. The mass spectrometry analysis of the samples was performed on a Bruker Compact Q-TOF high resolution Compact mass spectrophotometer. A 10µL of the sample was injected into the UHPLC and run through a loop at 50% Solvent A consisting of 0.1 % formic acid in H_2O (v/v) and 50% solvent B consisting of 0.1 % formic acid in Acetonitrile (v/v). The elemental analysis was recorded on flash 2000 organic elemental analyser.

2.2. Characterization

2.2.1. Electrochemical measurements

The cyclic voltammetric experiments for 0.002 $moldm^{-3}$ solutions of ferrocene compounds **L_1**, **L_4**, **L_5**, **L_9** and **L_{10}** were performed using Gamry Interface 1000 Potentiostat/Galvanostat/ZRA. The measurements of the samples were performed in three-electrodes workstation under two conditions with bare glassy carbon electrode(GCE) as the working electrode, a thin Pt wire as a counter electrode with Ag/AgCl reference electrode using 0.1 $mol^{-1}dm^{-3}$ tetrabutylammoniumhexafluorophosphate (*n*-Bu_4PF_6) as a supporting electrolyte in dichloromethane. The electrochemical test of **L_1**, **L_4**, **L_5**, **L_9** and **L_{10}** compounds was carried out

in dichloromethane CH_2Cl_2 solution in the dark and light illumination. Different scan rates were employed ranging from 20 to 80 mVs^{-1}. The bare glassy carbon electrode was thoroughly polished with a buffing pad after each experiment and washed with deionized water and sonicated for 30 min. The three-electrodes were suspended in a solution containing CH_2Cl_2.

2.2.2 General procedure for the synthesis of 3-nitrophenyferrocene

The full synthesis of the five reported 3-ferrocenylphenylimine compounds has been reported by Oladeji *et al*. [49]. They were subjected for further electrochemical characterization using cyclic voltammetry due to their high antimicrobial activities.

3-nitroaniline, 30 mL of concentrated hydrochloric acid and 30 mL of water were mixed together in a two-necked round bottom flask and cooled to ~0-5 ^oC in accordance to the procedure published by Ikhile *et al.* [42]. Thereafter, a specific amount of sodium nitrite solution was added dropwisely with stirring. The mixture was stirred further for an additional 30 min and kept at the temperature below 5^oC throughout this period. The mixed ferrocene and hexadecyltrimethylammonium bromide was added to 100 mL of diethyl ether and cooled to ~0-5 ^oC. The diazonium salt was added dropwisely and the mixture was stirred for additional ~5-6 h at room temperature. Lastly, the reaction mixture was extracted with dichloromethane and dried with dehydrated sodium sulphate and the crude extract was evaporated using rotary evaporator.

3-nitroaniline (13.4 g, 96.8 mmol), ferrocene (9.0 g, 48.37 mmol)) and sodium nitrite (9.0 g, 130.44 mmol) were used as the starting material in accordance to already published procedure [42] and other starting materials as stated above (section 2). The product was vacuum dried and gave an orange powder. The yield was 13.2 g, 90%, m.p.112.5 -112.9 ^oC; UV-Vis: 447 nm; FTIR ((KBr cm^{-1}): 3087, 2 937, 2864, 1 591, 1 519, 1 339, 1102, 1001, 890, 802, 741; ^1H (500 MHz, $CDCl_3$): δ(ppm): 8.23 (d, 1H, J = 7.8 Hz, C_6H_4), 8.01 (d, 1H, J = 7.8 Hz, C_6H_4), 7.76 (d, 1H, J = 7.8 Hz, C_6H_4), 7.53 (t, 1H, J = 8.1 Hz, C_6H_4) , 4.70 (s, 2H, C_5H_4), 4.39 (s, 2H, C_5H_4), 4.04 (s, 5H, C_5H_5), C (125 MHz, $CDCl_3$): δ(ppm) 148.5, 148.1, 142.1, 135.3, 134.7, 131.7, 130.4, 129.3, 123.8, 123.0, 121.6, 120.4, 120.3, 82.4, 69.9, 66.8; Anal. Calc. for $C_{16}H_{13}FeNO_2$ (%): EA: C, 62.59, H, 3.65, N, 4.61; Found (%): C, 62.98; H, 3.63; N, 4.59, Fe, 18.30, O, 10.49.

2.2.3 General procedure for the synthesis of 3-ferrocenylaniline

3-nitrophenylferrocene (4.02 g, 13.09 mmol) was added to 30 mL of concentrated hydrochloric acid and 40 mL of ethanol was added to granulated tin (8.82 g, 74.29 mmol) according to already published method [42]. The reaction mixture was heated at 700 rpm under reflux at 110 ^{o}C for 5 h. 150 mL of water was added together with NaOH after cooling the reaction to adjust the pH value to 14 and dark the mixture was filtered. The filtrate was extracted with water and dichloromethane (DCM) and the organic layer was dried with (Na_2SO_4). Rotary evaporation was used to remove the solvent. The concentrated crude was subjected to thin-layer chromatography using hex/DCM (50/50) and finally subjected to column chromatography as the eluent to give a pure compound.

3-nitrophenylferrocene (4.02 g, 13.09 mmol), granulated tin (8.82 g, 74.29 mmol) were used as the starting materials with other materials as stated above. (See Section 2.2). The product was vacuum dried and gave an orange powder. The yield was 2.1 g, 91%, m.p.128-128.5 ^{o}C, UV-Vis: 447 nm; FTIR ((KBr cm^{-1}): 3441, 3357, 3103, 2919, 2720, 1598, 1513, 1465, 1307, 1232, 1169, 1100, 999, 810; H (500 MHz, $CDCl_3$) δ(ppm): 7.13 (d, 1H, *J* = 7.8 Hz, C_6H_4), 6.96 (dd, 1H, *J* = 5.0 Hz, C_6H_4), 6.84 (s, 1H, C_6H_4), 6.56 (d, 1H, *J* = 7.8 Hz, C_6H_4), 4.62 (s, 2H, C_5H_4), 4.31 (s, 2H, C_5H_4), 4.08 (s, 5H, C_5H_5), 3.69 (s, 2H, -NH_2); δ C (125 MHz, $CDCl_3$): (ppm) 146.2, 140.2, 129.1, 117.0, 113.0, 112.8, 85.6, 69.5, 68.6, 66.5; Anal. Calc. for $C_{16}H_{15}FeN$ (%): EA: C, 69.12, H, 5.39, N, 5.08; Found (%): C, 69.34; H, 5.46; N, 5.05.

2.4. General procedure for the synthesis of ferrocenyl Schiff bases **(L_1, L_4, L_5, L_9, L_{10})**

An equal volume of 3-ferrocenylaniline and aromatic aldehyde were mixed together and dissolved with 15 mL dried ethanol in a two-necked flask equipped with a magnetic stirrer. The reaction was performed under reflux atmosphere and the mixture was heated for ~5-6 h. Thereafter, the thin layer chromatography TLC was used to determine the formation of **L_1-L_{10}** after ~5-6 h. Pressure vacuum was adopted to remove the solvent.

2.4.1 Synthesis of *N-(2,3-dimethoxy-benzylidene)-3-ferrocenylimine* **(L_1)`**

3-ferrocenylaniline (0.036 g, 0.21 mmol) and 2,3-dimethoxybenzaldehyde (0.034 g, 0.23 mmol). The product was collected as brownish colour powder: 0.0513 g, yield 63%, R_f 0.84, m.p. 240.5-

242.3 °C, UV-Vis (nm): 261, 304, 325, 454; FTIR (KBr cm^{-1}): 3088 (Ar[-]H), 2942, 2873, 2830, 2753, 1680 (CH=N), 1581 (C=C), 1475, 1384, 1311, 1258 (Cp), 1173 (*v*-C-O), 1068 (*v*-C-O), 996, 906, 784, 751 (Fe[-]Cp); ^{1}H(500 MHz, $CDCl_3$), δ(ppm): 10.46 (s, 1H, N=CH), 8.93 (s, 1H, C_6H_3); 7.80 (dd, 1H, *J* = 5.0 Hz, C_6H_3); 7.38 (d, 1H, *J* = 7.8 Hz, C_6H_3); 7.34 (t, 2H, *J* = 1.8 Hz, C_6H_3); 7.17 (t, 1H, *J* = 1.8 Hz, C_6H_3), 7.07 (dd, 1H, *J* = 5.0 Hz, C_6H_3); 4.71 (s, 2H, C_5H_4); 4.35 (s, 2H, C_5H_4); 4.09 (s, 5H, C_5H_5); 4.02 (s, 3H, OCH_3); 3.96 (s, 3H, OCH_3): ^{13}C (125 MHz, $CDCl_3$), δ(ppm): 190.1, 156.4, 153.0, 152.9, 150.2, 140.4, 129.9, 129.0, 124.3, 124.1, 123.7, 119.2, 119.0, 118.1, 117.9, 115.1, 85.0, 69.6, 68.9, 66.6, 56.0, 55.9; Anal. Calc. for $C_{25}H_{23}FeNO_2$, 425.3006; m/z HRMS (ESI): Found; 426.1102 (M^+ +1); Anal. Calc. for $C_{25}H_{23}FeNO_2$; Found (%): H, 5.54, C, 70.62, N, 3.19; EA (%) H, 5.45, C, 70.60, N, 3.29.

2.4.2 Synthesis of *N-(4-nitrobenzylidene)-3-ferrocenylimine* **(L_4)**

3-ferrocenylanline (0.040 g, 0.23 mmol) and 4-nitrobenzaldehyde (0.035 g, 0.23 mmol). The product was collected as gold colour powder: 0.0810 g, yield 86%, R_f 0.86, m.p. 330.5-332.5 °C, UV-Vis (nm): 287, 300, 352, 463; FTIR (KBr cm^{-1}): 3097 (Ar[-]H), 2934, 2853, 1702, 1660, 1511, 1338 (C-N), 1192, 1101, 1003 Cp, 840, 678 (Fe[-]Cp); ^{1}H(500 MHz, $CDCl_3$), δ(ppm): 10.19 (s, 1H, N=CH); 8.63 (s, 1H, C_6H_4); 8.40 (dd, 2H, *J* = 5.0 Hz, C_6H_4); 8.12 (dd, 2H, *J* = 5.0 Hz, C_6H_4); 7.45 (d, 1H, *J* = 7.8 Hz,C_6H_4); 7.37 (t, 1H, *J* = 1.8 Hz, C_6H_4); 7.10 (d, 1H, *J* = 7.8 Hz, C_6H_4), 4.72 (s, 2H, C_5H_4); 4.37 (s, 2H, C_5H_4); 4.09 (s, 5H, C_5H_5); ^{13}C (125 MHz, $CDCl_3$), δ(ppm): 190.1, 157.8, 151.1, 147.1, 141.6, 141.1, 140.8, 130.4, 129.4, 124.8, 124.3, 119.0, 84.57, 69.6, 69.1, 66.6; Anal. Calc. for $C_{23}H_{18}FeN_2O_2$, 410.2462; *m/z* HRMS (ESI): Found; 411.0511 (M^++1); Anal. Calc. for $C_{23}H_{18}FeN_2O_2$; Found (%): H, 4.68 C, 67.41, N, 6.72; EA (%) C, 67.34, H, 4.42, N, 6.83.

2.4.3 Synthesis of *N-(2-thiophenecarboxbenzylidene)-3-ferrocenylimine* **(L_5)**

3-ferrocenylanline (0.044 g, 0.25 mmol) and 2-thiophenecarboxaldehyde (0.034 mL, 170 mmol). The product was collected as faint yellow colour powder: 0.0701 g, yield 76%, R_f 0.73, m.p. 196.6-198.5 °C, UV-Vis (nm): 260, 300, 333, 461; FTIR (KBr cm^{-1}): 3099 (Ar[-]H), 2934, 2873, 2753, 1680 (N=CH), 1579 (C=C), 1430, 1384, 1264, 1183, 1069 Cp, 998, 906, 751C-S, 656 Fe[-]Cp); ^{1}H(500 MHz, $CDCl_3$), δ(ppm): 8.64 (s, 1H, N=CH), 7.55 (dd, 2H, *J* = 5.0 Hz, C_4H_5-S);

7.37 (dd, 1H, *J* = 5.0 Hz, C_6H_4); 7.34 (t, 2H, *J* = 1.8 Hz, C_6H_4), 7.18 (d, 1H, *J* = 7.8 Hz, C_6H_4); 7.06 (d, 1H, *J* = 7.8 Hz, C_6H_4); 4.71 (s, 2H, C_5H_4); 4.35 (s, 2H, C_5H_4); 4.08 (s, 5H, C_5H_4); ^{13}C (125 MHz, $CDCl_3$), δ(ppm): 152.9, 151.6, 142.9, 140.4, 132.1, 130.0, 129.0, 127.7, 123,6, 119.1, 69.6, 69.0, 66.5; Anal. Calc. for $C_{21}H_{17}FeNS$, 371.2764; *m/z* HRMS (ESI): Found; 372.0457 (M^++1); Anal. Calc. for $C_{21}H_{17}FeNS$; Found (%): H, 4.71, C, 67.91, N, 3.68; EA (%) H, 4.62, C, 67.93, N, 3.77.

2.4.4 Synthesis of *N-(3-nitrobenzylidene)-3-ferrocenylimine* **(L_9)**

3-ferrocenylanline (0.040 g, 0.23 mmol) and 3-nitrobenzaldehyde (0.035 g, 0.23 mmol). The product was collected as gold colour powder: 0.731 g, yield 78%, R_f 0.67, m.p. 335.5-337.5 ^oC, UV-Vis (nm): 259, 296, 328, 441; FTIR (KBr cm^{-1}): 3085 (Ar[-]H), 2936, 2853, 1701, 1665 CH=N, 1531, 1346 (NO_2), 1192, 1101, 1002 (CP), 841, 731 (Fc[-]Cp); ^1H(500 MHz, $CDCl_3$), δ(ppm): 10.19 (s, 1H, N=CH); 8.64 (s, 1H, C_6H_4); 8.40 (dd, 2H, *J* = 5.0 Hz, C_6H_4); 8.12 (dd, 2H, *J* = 5.0 Hz, C_6H_4); 7.55 (d, 1H, *J* = 8.7 Hz,C_6H_4); 7.36 (t, 1H, *J* = 1.8 Hz, C_6H_4); 7.10 (d, 1H, *J* = 7.8 Hz, C_6H_4), 4.72 (s, 2H, C_5H_4); 4.37 (s, 2H, C_5H_4); 4.09 (s, 5H, C_5H_5); ^{13}C (125 MHz, $CDCl_3$), δ(ppm): 189.6, 157.1, 151.0, 148.7, 140.8, 137.4, 134.5, 134.0, 130.3, 129.8, 124.6, 124.3, 119.0, 84.6, 69.6, 69.1, 66.6; Anal. Calc. for $C_{23}H_{18}FeN_2O_2$, 410.2462; mol. weight 410.07; *m/z* HRMS (ESI): Found; 411.0743 (M^+ +1); Anal. Calc. for $C_{23}H_{18}FeN_2O_2$; Found (%): H, 4.48 C, 67.41, N, 6.72; EA (%) C, 67.34, H, 4.42, N, 6.83.

2.4.5 Synthesis of *N-(2-furabenzylidene)-3-ferrocenylimine* **(L_{10})**

3-ferrocenylanline (0.096 g, 0.55 mmol) and 2-furaldehyde (0.092 g, 0.96 mmol). The product was collected as black colour powder: 0.1407 g, yield 76%, R_f 0.72, m.p. 193.5-195.2 ^oC; UV-Vis (nm): 259, 298, 329, 466; FTIR (KBr cm^{-1}): 3357 (C-O), 3092 (Ar[-]H), 2865, 1676 (CH=N), 1594, 1464, 1389, 1338, 1277, 1230, 1155, 1010 (Cp), 928, 882, 812, 749 (Fc[-]Cp); ^1H(500 MHz, $CDCl_3$), δ(ppm): 9.70 (s, 1H, N=CH); 8.37 (s, 1H, C_6H_4); 7.69 (d, 1H, *J* = 7.8 Hz, -OC_4H_3); 7.43 (t, 1H, *J* = 1.8 Hz, C_6H_4); 7.34 (t, 1H, *J* = 1.5 Hz, -OC_4H_3); 7.09 (dd, 1H, *J* = 5.0 Hz, -OC_4H_3); 6.61 (dd, 1H, *J* = 5.0 Hz, C_6H_4); 6.40 (d, 1H, *J* = 7.8 Hz, C_6H_4); 4.70 (s, 2H, C_5H_4); 4.35 (s, 2H, C_5H_4); 4.08 (s, 5H, C_5H_5); ^{13}C (125 MHz, $CDCl_3$), δ(ppm): 177.8, 153.0, 148.0, 147.6, 145.6, 140.5, 129.1, 124.0, 119.6, 117.4, 116.2, 112.5, 112.1, 69.6, 69.0, 66.5;

Anal. Calc. for $C_{21}H_{17}FeNO$, 355.2108; *m/z* HRMS (ESI): Found; 356.0679 (M^+ + 1); Anal. Calc. for $C_{21}H_{17}FeNO$; Found (%): H, 4.82, C, 70.80, N, 3.21; EA (%) H, 4.82, C, 71.01, N, 3.94.

3. Results and discussion

3.1 Photophysical and optical characterization

The 3-nitrophenylferrocene synthesis was a precursor of 3-ferrocenylphenylimine synthesis, which was carried out via arylation of ferrocene by diazonium salt under phase transfer condition, and the nitro derivatives were later reduced with Sn/HCl in order to acquire ferrocenylaniline (Scheme 1). Thereafter, the imine compounds were formed by reacting benzyl aldehydes with ferrocenylaniline as stated in (Scheme 2) which were performed under nitrogen condition. The obtained data indicate the absorption bands at 3441 cm^{-1} and 3357 cm^{-1} assigned to N-H stretching band of aniline on aromatic compounds. The band at 3103 cm^{-1} was attributed to the symmetric stretching band while the band at 2919 cm^{-1} absorption peaks was assigned to the C-H band of asymmetric stretching of aromatic compounds [42, 44]. The formations of the pure products were monitored using Thin-layer chromatography (TLC) in conjunction with Fourier Transformation Infrared Spectroscopy (FTIR).

Synthetic partway for the synthesis of 3-nitrophenylferrocene and 3-ferrocenylaniline

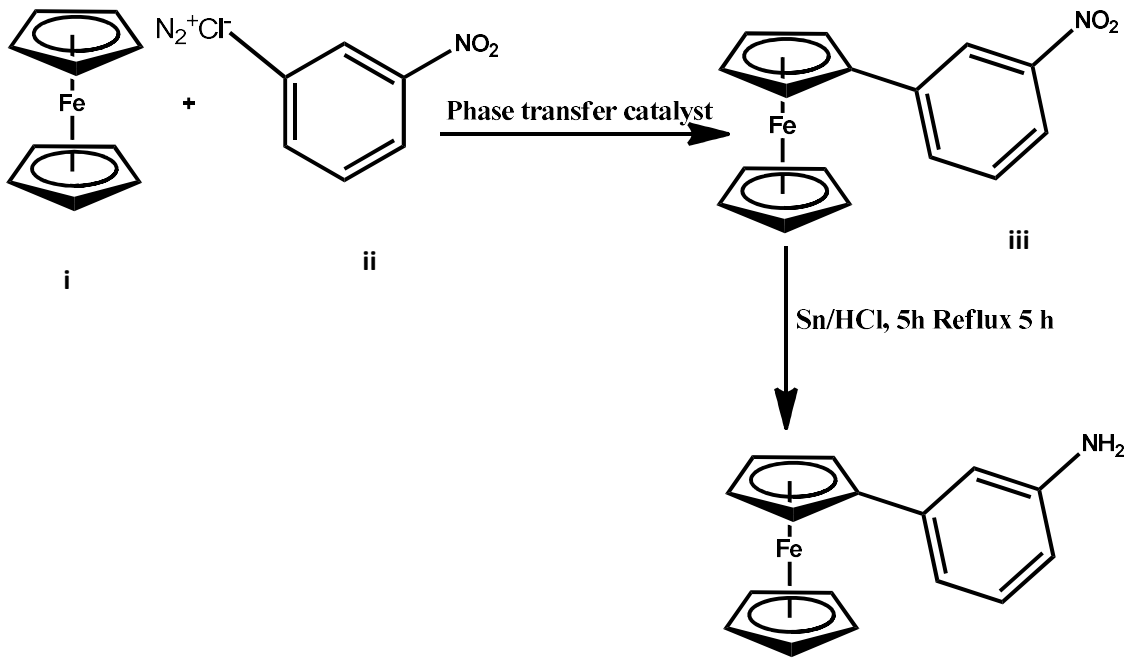

Scheme 1: Synthesis of 3-nitrophenylferrocene and 3-ferrocenylaniline

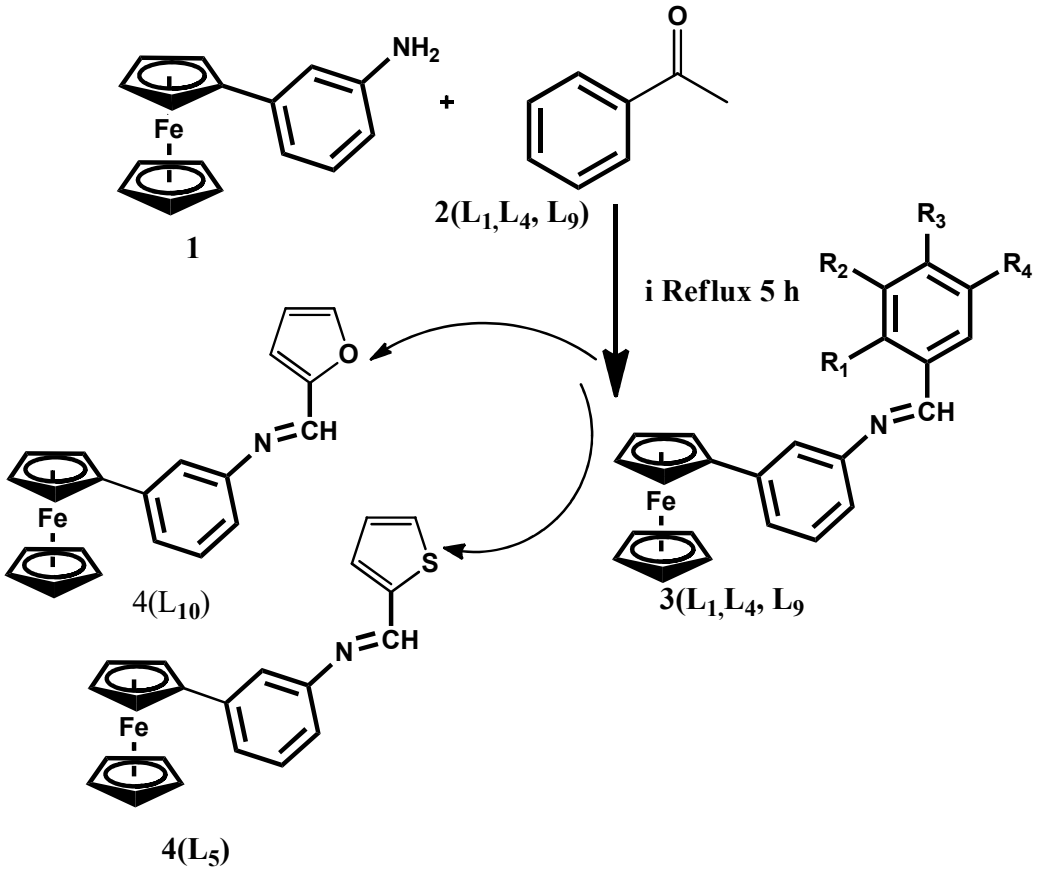

i. $R_1 = OCH_3$, $R_2 = OCH_3$, ii. $R_3 = NO_2$, iii. $R_1 = S$, iv. $R_2 = NO_2$, v. $R_3 = O$, $R_4 = H$

Scheme 2: Synthesis of 3-ferrocenylphenylimine (3-FPI) Schiff bases: (i) EtOH, Reflux 5 h.

We observe that ferrocenyl spectra indicated the absence of N-H and disappearance of C=O carbonyl stretching peak at around 1720 – 1712 cm^{-1} on aldehyde compound to the appearance of absorption at around 1680 - 1660 cm^{-1} which show the formation of C=N imine functional group (**i-v**) as shown in scheme **2**[42, 44]. The vibrational stretching of the C-N band for all ferrocenyl Schiff bases appeared around 1389 – 1337 cm^{-1}. The bands at 3099-3085 cm^{-1} absorption peaks are attributed to the C-H band of symmetric stretching while the bands at 1596-1527 cm^{-1} are corresponding to vibrational stretching of aromatic compounds. Table 1 shows the FTIR summary for the five compounds.

Table 1

Selected FTIR frequencies of compounds **L_1**, **L_4**, **L_5**, **L_9** and **L_{10}**

Compound	υ (C-N) (cm^{-1})	υ (C-H) (cm^{-1})	υ (C=C) (cm^{-1})	υ (C=N) (cm^{-1})
L_1	1383	3088	1580	1680
L_4	1337	3086	1596	1660
L_5	1384	3099	1579	1680
L_9	1346	3085	1527	1665
L_{10}	1389	3092	1594	1675

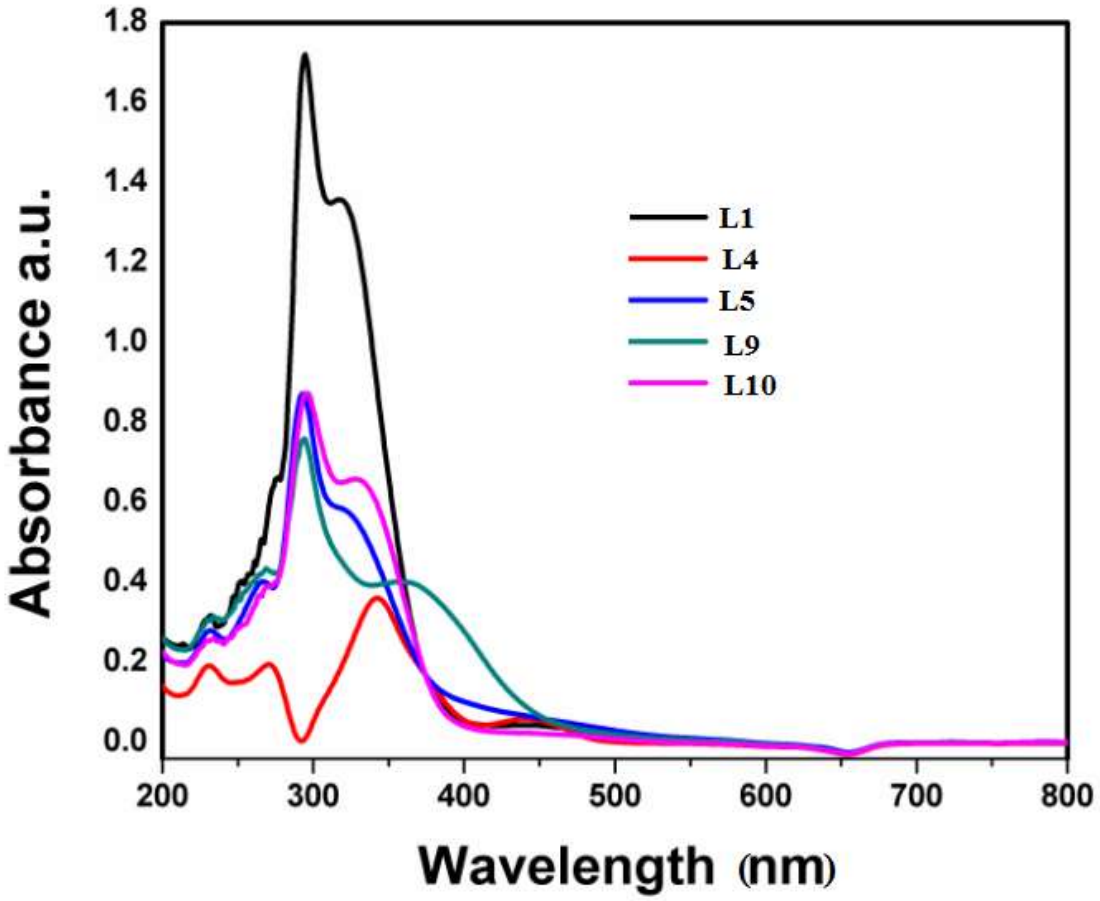

Fig. 1. UV-Vis absorption spectra of 0.002 $moldm^{-3}$ **L_1, L_4, L_5, L_9** and **L_{10}** in CH_2Cl_2.

Table 2

UV-Vis absorption data of **L_1**, **L_4**, **L_5**, **L_9** and **L_{10}** in dichloromethane

Compounds	Measured in CH_2Cl_2 (solvent)		
L_1	261	325	454
L_4	287	352	463
L_5	260	333	461
L_9	259	328	441
L_{10}	259	329	466

Absorption maxima λ in (nm) using 0.02 $moldm^{-3}$ solutions of ferrocene compounds

The ultra-violent visible spectroscopy analysis shown in Table 2 revealed three major absorptions range from 259-300 nm, 300-440 nm, and 441-466 nm. The first band is ascribed to the n-π* transition of the aromatic compound of Schiff bases. The second band give rise to intense bands between 300 - 340 nm and the absorption peaks are assigned to π- π* transition of metal-to-ligand charge transfer (MLCT) Fe(d)-Cp(π*) which allows the charge transportation from central cyclopentadienyl to be delocalized while the third absorption ranges between 441-466 nm corresponds to the d-d transition for the Fe of ferrocene which is similar to the results obtained by Thomas *et al*., 2011 on the analysis conducted in their publication of synthesis, UV/Vis spectra and electrochemical characterization of arylthio and styryl substituted ferrocenes [44, 54].

3.2 Cyclic voltammetry analysis

The electrochemical analyses of five compounds were determined using cyclic voltammetry which was performed in 0.002 $moldm^{-3}$ dichloromethane at room temperature (25 ^{0}C) and their corresponding electrochemical parameters are summarized in Table 3 & 4. Equal quantity of compounds was measured and the redox nature of **L_1**, **L_4**, **L_5**, **L_9** and **L_{10}** were determined by using glassy carbon electrode as a working electrode within a potential range of 0 to 1.00 V at scan rate 20 mV s^{-1} as shown in Fig. 2 (A - D). These five compounds were chosen due to their high potential antibacterial activities against the tested microbial strain [49]. An oxidation is observed at the anodic peak potential (Ep_a), indicating that the ferrocene moiety of the Schiff

base is converted to its oxidized form while the reduction of the oxidized product is occurring during the reverse scan and a cathodic signal is observed at the cathodic peak potential (Ep_c). The pure ferrocene redox couple values are 0.057 and 0.061 ± 0.02 V on GI 1000 Potentiostat/Galvanostat electrode in non-aqueous system. The cyclic voltammograms of compounds **L_1**, **L_4**, **L_5**, **L_9** and **L_{10}** ferrocenylphenylimine showed much consistent to these values and also showed a clear well-defined redox peak in both conditions (Light and dark). Fig. 6.2A showed the redox peaks of **L_4** and **L_{10}**, respectively in which the peak current of compound **L_{10}** increases slightly and peak potential also shifted only to the small extent due to the presence of N and O and conjugation π-bond. The cyclic voltammograms of ferrocenylphenylimine compounds of **L_5**, **L_9** and **L_1** were recorded in Fig. 2B. Among them, **L_9** compound showed a little increased peak current and slightly shifted the peak potential compared with **L_1** and **L_5**, this could be ascribed to the introduction of an electron-withdrawing effect of the nitro group on the benzene ring. The slight deviation is also ascribed to the attached Schiff bases to the structure [55]. **L_1** also showed a good redox peak current and peak potential in similarity compared with **L_5** as shown in Fig. 2B. Compound **L_5** show well redox peak current and peak potential compared to both **L_1** and **L_9**, which is attributed to intra-molecular hydrogen bonding between carboxyl and sulphur groups in its aromatic ring. Their similarities in peak current and peak potential under different condition is attributed to the stability of ferrocene/ferrocenium redox couple in dichloromethane.

Table 3

Cyclic voltammetry data of compounds **L_1**, **L_4**, **L_5**, **L_9** and **L_{10}** carried out in the presence of light illumination revealing cathodic and anodic peaks potential (E_{Pa} and E_{Pc}) and peak current (i_{Pa} and i_{Pc}) respectively at 20 mV/s.

Compounds	E_{Pa} (V)	E_{Pc} (V)	$E_{1/2}$ (V)	ΔE_P (V)
Ferrocene	0.034	-0.023	0.005	0.057
L_1	0.034	0.027	0.031	0.012
L_4	0.032	0.018	0.025	0.014
L_5	0.059	0.039	0.049	0.020
L_9	0.069	0.045	0.057	0.024
L_{10}	0.075	0.034	0.055	0.041

$E_{1/2} = (E_{pa} + E_{pc})/2$, $\Delta E_p = (E_{pa} - E_{pc})$, $E^0 = E_{1/2}$ (for a reversible reaction) using 0.002 mol dm^{-3} solutions of ferrocene compounds in CH_2Cl_2 at room temperature.

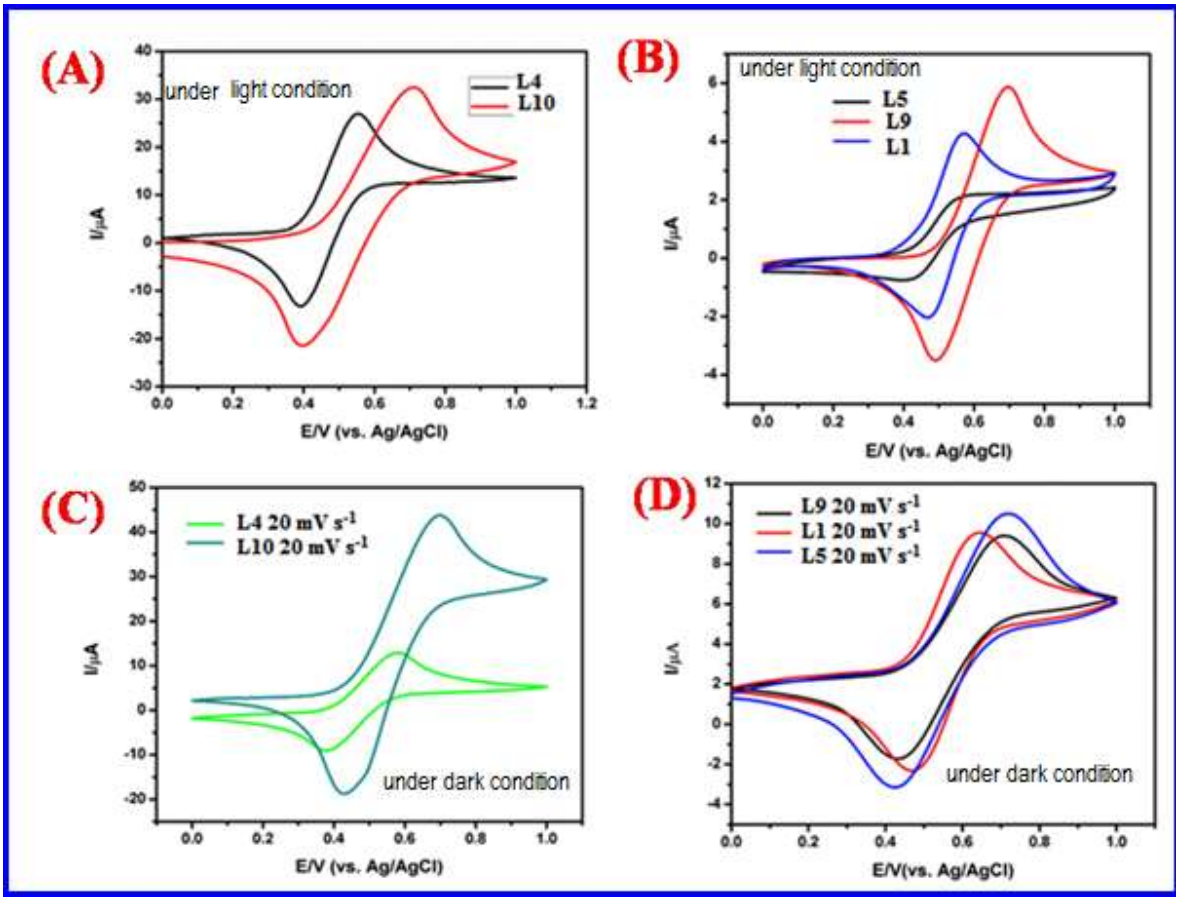

Fig. 2A-D. Cyclic voltammograms of **L_1**, **L_4**, **L_5**, **L_9** and **L_{10}** ferrocenylphenylimine at 20 mV/s scan rate under visible light and dark condition in 0.002 $mol^{-1}dm^{-3}$ CH_2Cl_2 at room temperature.

From Fig. 2 (A&B), the process was reversible and Fig. 3 (A&B) also has a similar shape. The peak separations potential in Fig. 2 (A&B) were observed to be lower compared to the peak separation potential of the standard ferrocene at 0.057 V and 0.061 V for light and dark conditions. These values (0.057 V and 0.061 V) indicate an ideal value for one electron oxidation. The lower peak separation values of **L_1**, **L_4**, **L_5**, **L_9** and **L_{10}** indicating a fast electron transfer which could be attributed to the presence of electron donating and withdrawing substituents in the structure. The cyclic voltammetry data of **L_1**, **L_4**, **L_5**, **L_9** and **L_{10}** were listed in Table 3 and the peak separation ΔE_P (V) values were found to be in the range between 0.011 – 0.041 V. A similar trend was also observed in Table 4 having a peak separation ΔE_P (V) values range between 0.020 – 0.031 V. Compound **L_1** and **L_5** in Fig. 2 (C&D) under complete darkness experience a positive shift compared to **L_4**, **L_9** and **L_{10}**. This was ascribed to the electron-

donating ability of methoxy –CH_3O and sulphur group attached to ferrocene body core structure which further speed the oxidation process by lowering E_{pa} [37]. Peak separation ΔE_P value indicate the level of electron transfer resistance that each of the compounds experienced. The higher the ΔE_P value, the greater the charge transfers resistance. With this effect, compound **L_1** under both conditions had the least peak separation ΔE_P = 0.011V and 0.020 V value, indicating the compound with the lowest electrons transfer resistance which is ascribed to the presence of electron-donating ability of methoxy group.

However, it was generally observed that there was no significant variation in the peak separation ΔE_P (V) values between the two conditions and it is attributed to the stability of ferrocenylphenylimine compounds **L_1**, **L_4**, **L_5**, **L_9** and **L_{10}**. The ratio of the cathodic to anodic peak current (ip_a/ip_c) equal to unity for compounds **L_1, L_9** and **L_{10}** under the influence of light radiation as shown in Table 6 (1.004, 1.031 and 1.083) while **L_4** and **L_5** peak current remained nearly equal to unity which indicates a reversible and quasi-reversible reaction and was found independent of the scan rate. Similar results were observed for compounds **L_1**, **L_4**, **L_5**, **L_9** and **L_{10}** in dark condition with peak currents of 0.995, 1.019, 1.046, 1.190 and 1.037 as shown in Table 8 these results indicated that the oxidized form is stable within the time frame of the experiment and the charge-transfer process is reversible.

Half-wave potential $E_{1/2}$was carried out for the ferrocene standard to determine its response to oxidation and reduction. The response shows that ferrocene had a potential value of ($E_{1/2}$ = 0.004 V) which is lower than the potentials exhibited by the five compounds with their peaks potential value range between (0.031 V to 0.057 V) at 20 mV/s under light illumination and (0.028 V to 0.041 V) in dark condition. These potentials are anodically shifted when compared to the potential of ferrocene [42- 44].

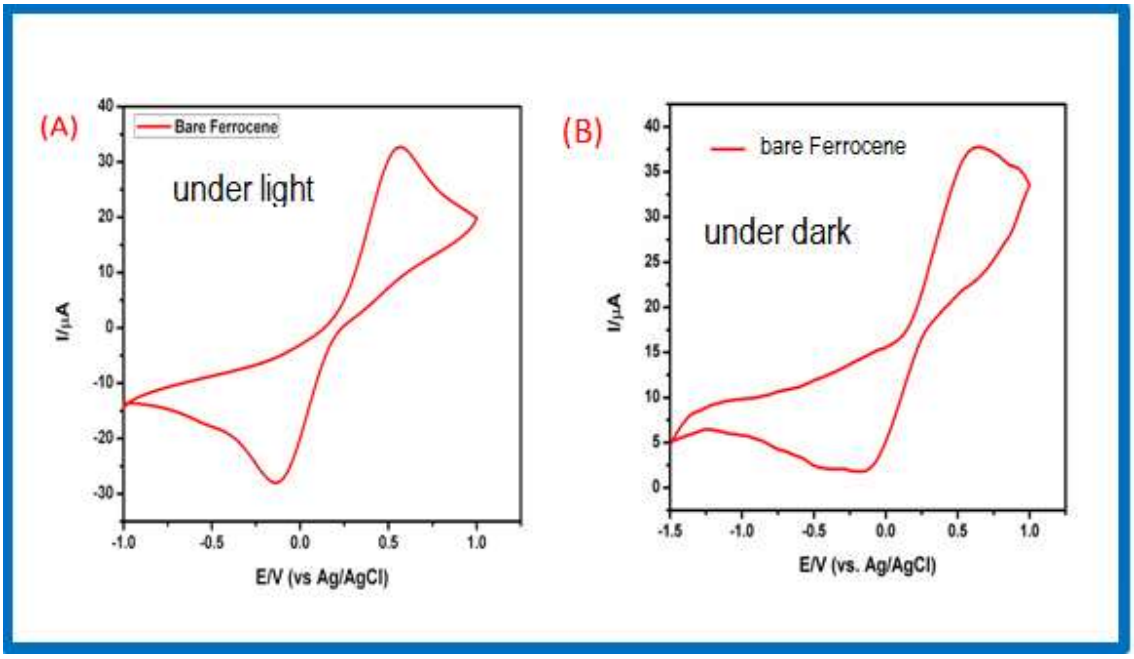

Fig. 3A&B. Cyclic voltammograms of bare ferrocene at 20 mV/s scan rate under visible light and dark condition in 0.002 moldm^{-3} CH_2Cl_2 at room temperature.

Table 4

Cyclic voltammetry data of compounds **L_1**, **L_4**, **L_5**, **L_9** and **L_{10}** carried out in the dark revealing cathodic and anodic peaks potential (E_{pa} and E_{pc}) and peak current (i_{pa} and i_{pc}) respectively.

Compounds	E_{pa} (V)	E_{pc} (V)	$E_{1/2}$ (V)	ΔE_p (V)
Ferrocene	0.040	-0.021	0.008	0.061
L_1	0.049	0.029	0.039	0.020
L_4	0.039	0.017	0.028	0.022
L_5	0.055	0.024	0.041	0.031
L_9	0.051	0.022	0.036	0.029
L_{10}	0.049	0.021	0.035	0.027

$E_{1/2}$= (E_{pa} + E_{pc})/2, ΔE_p = (E_{pa} – E_{pc}), E^0 = $E_{1/2}$ (for a reversible reaction), in 0.002 moldm^{-3} CH_2Cl_2 at room temperature

3.3 Effects of different scan rate

The effect of different scan rate on the redox activities of compounds **L_1**, **L_4**, **L_5**, **L_9** and **L_{10}** in 0.002 moldm^{-3} CH_2Cl_2 at room temperature using three-electrodes system were investigated under light and dark condition as shown in Fig. 4&6. The system displayed reversible behaviours confirming its earlier discussion. Furthermore, the scan rate study helped to confirm both the diffusion coefficient and adsorption controlled nature of the reactions. The linear plot of different scan rate versus peak current was observed in compounds **L_1**, **L_4**, **L_5**, **L_9** and **L_{10}**. The correlation coefficient of i_{pa} and i_{pc} for **L_1** (R^2 =0.98697, 0.9978), **L_4** (R^2 = 0.9684, 0.97623), **L_5** (R^2 = 0.97435, 0.90742) and **L_9** (R^2 = 0.9945, 0.908) and **L_{10}** (R^2 = 0.97, 0.976) have been calculated using the Randles-Sevcik equation and they are well fitted as depicted in Fig. 5 (A-E). The calibration plots values of diffusion coefficient showed that the electron transfer process is diffusion controlled reaction for all the compounds. The variation in scan rate in all the five compounds has no significant effect which is ascribed to their stability as peak potentials undergo reversibility processes except for compounds **L_5** and **L_9** Fig. 4 (C&D) in the presence of visible light that experienced a quasi-reversible. A reverse situation was experienced with half-wave potential $E_{1/2}$ that decreases with increase in scan rate. Compound **L_4** had the least $E_{1/2}$ value compared to other compounds because of the effect of nitro group on the aromatic compound.

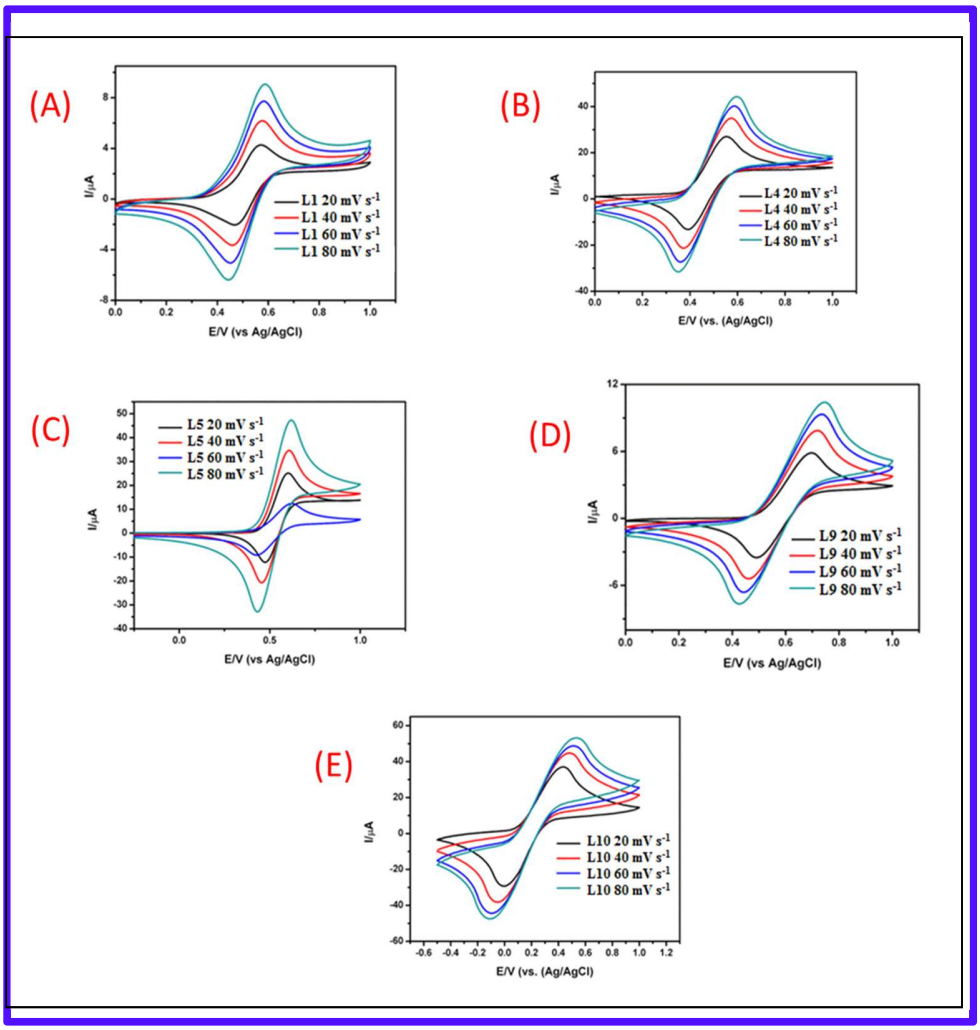

Fig. 4 (A-E). Cyclic voltammograms of compounds **L_1**, **L_4**, **L_5**, **L_9** and**L_{10}** in the presence of visible light with bare GCE, Pt counter electrode and Ag/AgCl reference electrode in 0.1 moldm^{-3} Bu_4NPF_6 supporting electrode with different scans rate ranging from 20 to 80 mV s^{-1} in 0.002 moldm^{-3} CH_2Cl_2 at room temperature,

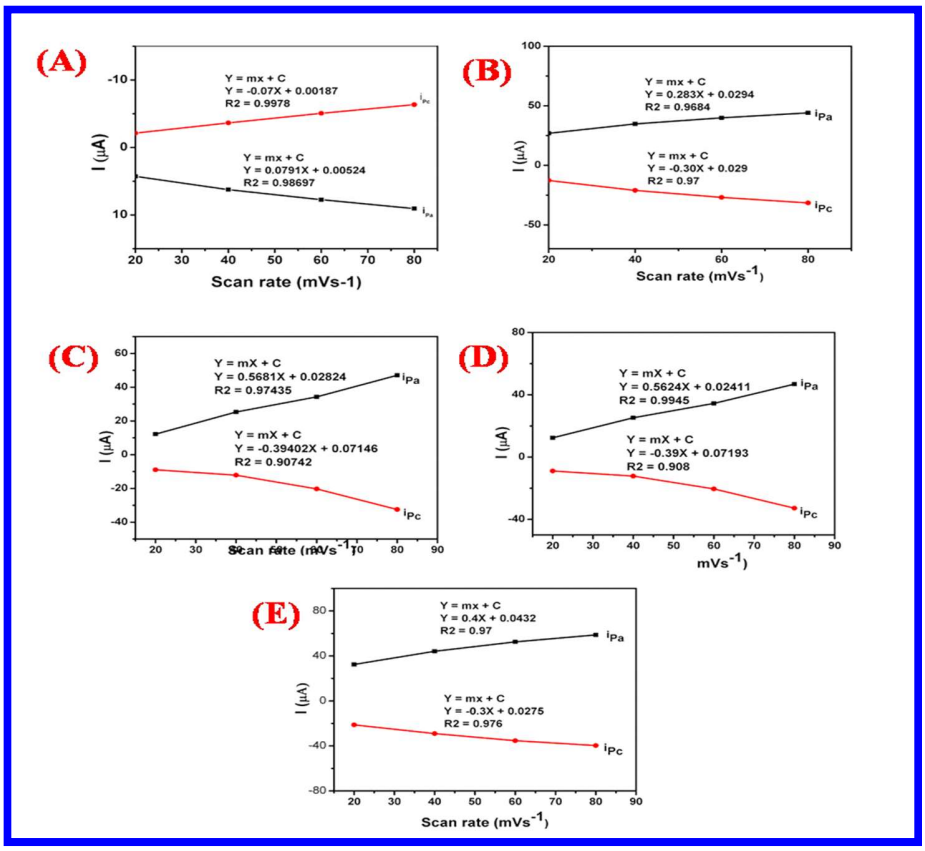

Fig. 5 (A-E). Calibration plots of (A) **L_1**, (B) **L_4**, (C) **L_5**, (D) **L_9** and (E) **L_{10}** under light condition in 0.002 moldm^{-3} CH_2Cl_2 at room temperature

Table 5

Cyclic voltammetry data of compounds **L_1**, **L_4**, **L_5**, **L_9** and **L_{10}** carried out in the presence of light using different scan rate showing anodic and cathodic potential peaks (E_{pa} and E_{pc}) together with half-wave potential and potential separation ($E_{1/2}$ and ΔE_p) respectively.

Cmd	**Scan rates**											
	40 (V)				**60 (V)**				**80 (V)**			
	E_{pa}	E_{pc}	$E_{1/2}$	ΔE_p	E_{pa}	E_{pc}	$E_{1/2}$	ΔE_p	E_{pa}	E_{pc}	$E_{1/2}$	ΔE_p
L_1	0.049	0.029	0.039	0.020	0.045	0.023	0.033	0.022	0.048	0.024	0.036	0.024
L_4	0.042	0.017	0.029	0.025	0.048	0.015	0.031	0.033	0.049	0.013	0.031	0.036
L_5	0.057	0.027	0.042	0.031	0.051	0.024	0.037	0.027	0.052	0.024	0.038	0.028
L_9	0.062	0.021	0.041	0.041	0.062	0.024	0.043	0.038	0.067	0.024	0.045	0.043
L_{10}	0.067	0.013	0.040	0.054	0.067	0.013	0.040	0.054	0.067	0.013	0.040	0.054

Cmd indicates compound, $E_{1/2} = (E_{pa} + E_{pc})/2$, $\Delta E_p = (E_{pa} - E_{pc})$, $E^0 = E_{1/2}$ (for a reversible reaction) in 0.002 moldm^{-3} CH_2Cl_2 at room temperature

Table 6

Cyclic voltammetry data of compounds **L_1**, **L_4**, **L_5**, **L_9** and **L_{10}** carried out in the presence of light using 20 to 80 mV/s scan rates showing anodic peak current and cathodic peak current ($\boldsymbol{i_{Pa}}$ and $\boldsymbol{i_{Pc}}$) respectively.

Scan rate	20 (mV/s)			40 (mV/s)			60 (mV/s)			80 (mV/s)		
Com	$\boldsymbol{i_{Pa}}$ (µA)	$\boldsymbol{i_{Pc}}$ (µA)	$\mathbf{i_{pc}/i_{pa}}$	$\boldsymbol{i_{Pa}}$ (µA)	$\boldsymbol{i_{Pc}}$ (µA)	$\mathbf{i_{pc}/i_{pa}}$	$\boldsymbol{i_{Pa}}$ (µA)	$\boldsymbol{i_{Pc}}$ (µA)	$\mathbf{i_{pc}/i_{pa}}$	$\boldsymbol{i_{Pa}}$ (µA)	$\boldsymbol{i_{Pc}}$ (µA)	$\mathbf{i_{pc}/i_{pa}}$
L_1	4.262	4.280	1.004	7.730	9.234	1.194	7.997	10.232	1.267	11.235	12.144	1.080
L_4	25.485	24.912	0.977	33.012	36.126	1.094	36.824	39.731	1.078	41.217	44.331	1.075
L_5	10.626	9.013	0.848	10.086	10.235	1.014	12.923	11.613	0.898	14.374	15.817	1.100
L_9	5.836	6.019	1.031	8.246	8.355	1.013	9.929	9.928	0.999	11.328	11.310	0.998
L_{10}	32.054	34.473	1.083	41.235	41.384	1.003	59.214	60.447	1.020	66.445	69.357	1.043

Com, represents compound

However, when the experiment was repeated in the dark condition using the same electrode and a similar trend was observed as shown in Fig. 6 (A-E). The calibration plot of different scan rate versus peak current was observed for **L_1**, **L_4**, **L_5**, **L_9** and **L_{10}** as revealed in Fig. 7 (A-E). The correlation coefficient of i_{Pa} and i_{Pc} for **L_1** (R^2 =0.98, 0.999), **L_4** (R^2 = 0.966, 0.9684), **L_5** (R^2 = 0.97459, 0.96235) and **L_9** (R^2 = 0.97435, 0.95645) and **L_{10}** (R^2 = 0.97, 0.963) are well fitted and as depicted the electron transfer process is diffusion controlled process [55]. We have observed a similar behaviour for light condition in the previous discussion and with dark condition; it further confirmed that a change in the scan rate had no significant effect as a result of their stability in non-aqueous system within the time frame of the experiment as shown in Table 5. Most of the peak currents were up to unity except compound **L_9** which is an indication of a reversible and quasi-reversible process as shown in Table 8. The effects of the strong electron-withdrawing nitro substituent of **L_4** cyclopentadienyl ring facilitate oxidation difficulties by making oxidation potential shift to a more negative direction. This attribute tells that the electrochemical oxidation behaviour of oxidizing ferrocene moiety depending on the electronic properties of the substituent

close to cyclopentadienyl ring [5]. This report was similar to the formerly reported on Schiff bases compounds bearing ferrocene moiety [43, 44]. The effect of half-have potential $E_{1/2}$ correlate with that of light condition as most of the compounds especially the electron-withdrawing substituents increases as the scan rate increases (**L_4**, **L_5** and **L_9**), while **L_1** and **L_{10}** compounds decrease with the increasing scan rate based on their carbon-nitrogen double bond effect (C=N) as well as the presence of heteroatom oxygen (C=O) on aromatic compound.

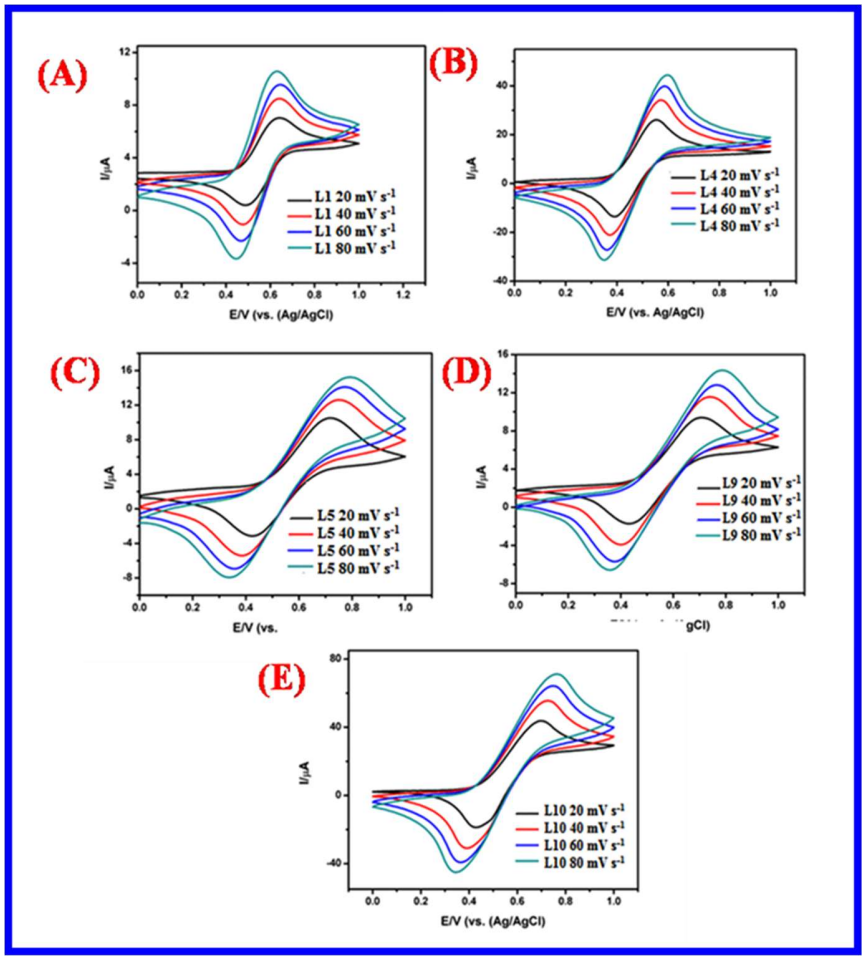

Figure 6 (A-E) Cyclic voltammograms of compounds **L_1**, **L_4**, **L_5**, **L_9** and**L_{10}** in the dark with bare GCE, Pt counter electrode and Ag/AgCl reference electrode in 0.1 M Bu_4NPF_6 supporting electrode with different scans rate ranging from 20 to 80 mV s^{-1} in CH_2Cl_2.

Table 7

Cyclic voltammetry data of compounds **L_1**, **L_4**, **L_5**, **L_9** and **L_{10}** carried out in the dark using different scan rates range between 20 - 80 mV/s showing anodic and cathodic potential peaks (E_{Pa} and E_{Pc}) together with half potential and potential separation ($E_{1/2}$ and ΔE_P) respectively.

Cmd	**Scan rates**											
	40 (V)				**60 (V)**				**80 (V)**			
	E_{Pa}	E_{Pc}	$E_{1/2}$	ΔE_P	E_{Pa}	E_{Pc}	$E_{1/2}$	ΔE_P	E_{Pa}	E_{Pc}	$E_{1/2}$	ΔE_P
L_1	0.063	0.024	0.043	0.039	0.064	0.027	0.045	0.037	0.062	0.024	0.043	0.038
L_4	0.057	0.013	0.033	0.044	0.058	0.015	0.036	0.043	0.059	0.014	0.036	0.045
L_5	0.075	0.015	0.045	0.060	0.074	0.015	0.044	0.059	0.075	0.013	0.044	0.062
L_9	0.074	0.017	0.046	0.057	0.076	0.017	0.093	0.059	0.078	0.015	0.046	0.063
L_{10}	0.072	0.019	0.045	0.053	0.074	0.016	0.090	0.058	0.076	0.014	0.045	0.062

Cmd represents compound, $E_{1/2} = (E_{pa} + E_{pc})/2$, $\Delta E_p = (E_{pa} - E_{pc})$, $E^0 = E_{1/2}$ (for a reversible reaction) in 0.002 moldm^{-3} CH_2Cl_2 at room temperature

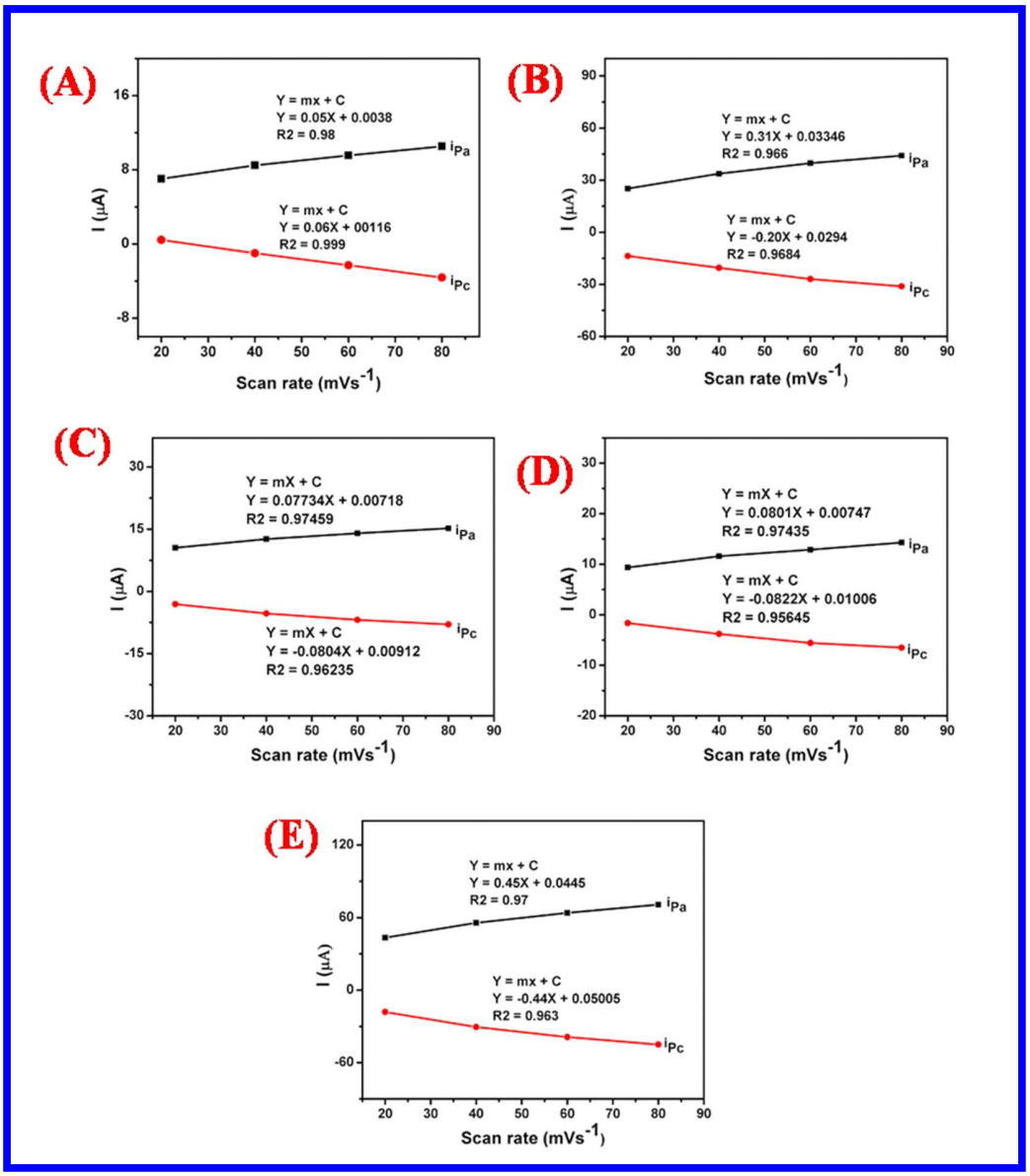

Figure 7: Calibration plots of (A) **L**$_1$, (B) **L**$_4$, (C) **L**$_5$, (D) **L**$_9$ and (E) **L**$_{10}$ under dark condition

Table 8

Cyclic voltammetry data of compounds **L_1**, **L_4**, **L_5**, **L_9** and **L_{10}** carried out in dark condition using 20 to 80 mV/s scan rates showing anodic peak current and cathodic peak current (i_{Pa} and i_{Pc}) respectively

Scan rate	20 (mV/s)			40 (mV/s)			60 (mV/s)			80 (mV/s)		
Com	i_{Pa} **(μA)**	i_{Pc} **(μA)**	**i_{pc}/i_{pa}**	i_{Pa} **(μA)**	i_{Pc} **(μA)**	**i_{pc}/i_{pa}**	i_{Pa} **(μA)**	i_{Pc} **(μA)**	**i_{pc}/i_{pa}**	i_{Pa} **(μA)**	i_{Pc} **(μA)**	**i_{pc}/i_{pa}**
L_1	4.170	4.173	1.000	6.069	6.071	1.000	7.259	7.504	1.033	8.793	9.143	1.039
L_4	24.658	25.131	1.019	33.116	34.936	1.054	37.945	39.658	1.045	41.008	44.331	1.081
L_5	7.879	8.246	1.046	10.863	11.719	1.078	13.097	14.259	1.088	14.398	15.928	1.106
L_9	7.308	8.701	1.190	13.460	11.054	0.821	13.953	12.206	0.874	15.660	14.015	0.894
L_{10}	40.623	42.140	1.037	53.934	55.964	1.037	66.021	67.918	1.028	74.514	77.353	1.038

Table 9

HOMO-LUMO energy level and band gap for compounds **L_1**, **L_4**, **L_5**, **L_9**, and **L_{10}** in the presence of visible light radiation.

Compound	Homo (eV)	Lumo (eV)	E_g (eV)
L_1	-5.370	-2.320	3.050
L_4	-5.349	-2.477	2.872
L_5	-5.395	-2.422	2.973
L_9	-5.495	-2.490	3.005
L_{10}	-5.194	-2.140	3.054

HOMO = -[4.8$_{eV}$ - E_{ox} (vs.Fc/Fc$^+$)], oxidation peak is indicated as E_{OX}, Lumo is given as Homo + E_g, the band gap is indicated as E_g and calculated from absorption intercept spectra.

Result of the highest occupied molecular orbital HOMO and the lowest unoccupied molecular orbital LUMO energy experiment carried out in the presence and absence of visible light with Ag/AgCl electrode is tabulated in Table 9 and 10. The HOMO energy level in the presence of light appears in the range of -5.194 to -5.495 in order of $\mathbf{L_9} < \mathbf{L_5} < \mathbf{L_1} < \mathbf{L_4} < \mathbf{L_{10}}$ while the HOMO energy level in the absence of light range from -5.352 to – 5.516 eV in order of $\mathbf{L_5} < \mathbf{L_9} < \mathbf{L_{10}} < \mathbf{L_1} < \mathbf{L_4}$. The HOMO-LUMO energy levels are very important parameters in the evaluation of energy performance as they indicate the possibility of effective electron transfer and dye regeneration. According to Chaiamornnugool *et al*. [45] and Kotteswaran *et al*. [46], for efficient transfer of electrons from oxidised dye into the conduction band of semiconductor TiO_2 to take place, the LUMO energy level of the dye must be greater than the conduction band edge of TiO_2 (-0.5 V vs. SCE). The HOMO energy level of the dye must be lower than the iodine/triiodide redox couple (0.4 V vs. SCE) [46]. The obtained HOMO energy level of all the five compounds $\mathbf{L_1}$, $\mathbf{L_4}$, $\mathbf{L_5}$, $\mathbf{L_9}$, $\mathbf{L_{10}}$ investigated were sufficient for effective dye regeneration which agreed with [47] report. They are lower than the HOMO energy level of iodine/triiodide redox couple. However, contrary to our expectation, the LUMO energy levels of all the five compounds carried out in the visible light and in the absence of visible light were slightly lower as compared to the LUMO energy level of the conduction band edge of TiO_2 (-0.5 V vs. SCE). This is necessary to facilitate the efficient electrons injection into the conduction band edge of the semiconductor. They are in order of $\mathbf{L_{10}} > \mathbf{L_1} > \mathbf{L_5} > \mathbf{L_4} > \mathbf{L_9}$ while the absence of visible light give the LUMO energy level which followed the order of $\mathbf{L_1} > \mathbf{L_{10}} > \mathbf{L_5} > \mathbf{L_4} > \mathbf{L_9}$. However, there were lower values of HOMO-LUMO energy level as shown in Table 10 when compared to Table 9, which implies faster regeneration of oxidized dye. Compounds $\mathbf{L_9}$ and $\mathbf{L_5}$ (-0.5495 and -5.516 eV) had the lowest HOMO energy level while $\mathbf{L_1}$ and $\mathbf{L_{10}}$ compounds had the highest LUMO energy level (-2.389 and -2.140 eV) that could be attributed to their electron-donating ability which implies good thermodynamic condition for efficient electrons transportation and regeneration over other compounds.

Table 10

HOMO-LUMO energy level and band gap for compounds **L_1**, **L_4**, **L_5**, **L_9**, and **L_{10}** in the dark (absence of visible light) using aqueous electrode

Compound	Homo (eV)	Lumo (eV)	E_g (eV)
L_1	-5.439	-2.389	3.050
L_4	-5.352	-2.480	2.872
L_5	-5.516	-2.543	2.973
L_9	-5.502	-2.497	3.005
L_{10}	-5.496	-2.442	3.054

HOMO = -[4.8_{eV} - E_{ox}($vs.$ Fc/Fc^+)], oxidation peak is indicated as E_{ox}, -4.8 eV is the energy level of Fc/Fc^+ relative to the vacuum energy level, Lumo is given as Homo + E_g eV, band gap is indicated as E_g and calculated from absorption intercept spectra.

4. Conclusion

Five compounds of 3-ferrocenylphenylimne derivatives were successfully synthesized, characterized by various techniques and investigates for electrochemistry analysis. Cyclic voltammetry results reveal good redox behaviour of all tested compounds under different conditions. The change in the scan rates from 20-80 mVs^{-1} in 0.002 $moldm^{-3}$ CH_2Cl_2 at room temperature does not show significant effect, as many peak potentials undergo reversible processes. All five compounds increase in current peak i_{Pa} and i_{Pc} under both conditions with increasing scan rates and produced nearly up to unity. Dark experiment showed similar potential peak currents when compared to the light experiment. Compound **L_5** had the lowest HOMO energy level (-5.516 eV) while compound **L_1** displayed the highest LUMO energy level (-2.140 eV) in the presence of visible light. All the five 3-ferrocenylphenylimine compounds carried out under both conditions tend to give better LUMO energy value that facilitate better electrons transportation with little variation. Both conditions displayed better potential peak currents and the highest peak current was achieved with compound **L_{10}** in dark condition. Compound **L_9** also showed the highest half-wave potential $E_{1/2}$ (0.057 V) while compound **L_1** showed the lowest

potential separation ΔE_P (0.011 V) in the presence of visible light. Generally, the analysis conducted under both conditions shows efficient performance indicate the stability of the ferrocenyl compounds in non-aqueous system as there is no significant difference in their behaviours under both conditions.

Conflict of interest

There is no conflict of interest among the authors

Acknowledgments

All the authors are very grateful to the Department of Chemical Sciences, the University of Johannesburg for their financial support and providing an enabling condition to carry out this project.

REFERENCES

1. T. J. Kealy, P. L. Pauson, Nature, 165 (1951**)** 1039–1040.
2. S. A. Miller, J. A. Tebboth, J .F. Tremaine, J. Chem. Soc. (1952) 632–635.
3. G. Wilkinson, M. Rosenblum, M. Whiting, R.B. Woodward, J. Am. Chem. Soc. 74 (1952) 2125–2126.
4. J. D. Dunitz, L. E. Orgel, Nature, 168 (1953) 121– 122.
5. T. Mermer, Y. Keles, N. Sirin, J. Biooga. Chem. 114 (2021) 105076.
6. H. Werner, Angew. Chem., Int. Ed., 51 (2012) 6052–6058.
7. D. R. Van Staveren, N. Metzler-Nolte, Chem. Rev. 104 (2004) 5931–5.
8. P. F. Eiland, R. Pepinsky, J. Am. Chem. Soc. 74 (1952) 4971–4971.
9. A. Togni, John Wiley & Sons, New York, (2008) 433–46.
10. D. Schaarschmidt, H. Lang, Organomet. 32 (2013) 5668.
11. D. Astruc, Pure Appl. Chem. 75 (2003) 461.
12. M. Drusan, R. Sebesta, Tetrahedron, 70 (2014) 759.
13. L-X. Dai, T. Tu, S-L. You, W-P. Deng, X-L. Hou, Acc. Chem. Res.36 (2003) 659.
14. D. Schaarschmidt, H. Lang, Eur. J. Inorg. Chem. 2010 (2010) 4811.
15. D. Schaarschmidt, H. P. Lang, ACS Catal. 1 (2011) 41.

16. S. Sansook, S. Hassell-Hart, C. Ocasio, J. Spencer, J. Organom. Chem. 905 (2020) 121017.
17. S. Barlow, D. O'Hare, Chem. Rev. 97 (1997) 637.
18. A. Ceccon, S. Santi, L. Orian, A. Bisello, Coord. Chem. Rev. 248 (2004) 683.
19. F. Paul, C. Lapinte, Coord. Chem. Rev. 431 (1998) 178-180.
20. A. Hildebrandt, H. Lang, Organomet. 32 (2013**)** 5640.
21. J. Rajput, A. T. Hutton, J. R. Moss, H. Su, C. Imrie, J. Organomet. Chem. 691 (2006) 4573–4588.
22. S. Park, V. K. Mathur, R. P. Planap, Polyhedron. 17 (1998) 325.
23. C. Imrie, P. Engelbrecht, C. Loubser, C. W. McCleland, V. O. Nyamoria, R. Bogardi, D. C Levendis, N. Tolom, J. Rooyen, N. Williams, J. Organomet. Chem. 645 (2002) 65–81.
24. L. F. Landy (Ed.), Cambridge, 1989.
25. Y. K. Choi, W. S. Kim, K. I. Chung, M. W. Chung, H. P. Nam, Microchem. J. 65 (2000) 3.
26. J. R. Aranzaes, M-C. Daniel, D. A. Can, J. Chem. 84 (2006) 288.
27. Y. Yu, A. D. Bond, P. W. Leonard, U. J. Lorenz, T. V. Timofeeva, K. P. Vollhardt, G. D. Whitener, A. A. Yakovenko, Chem. Commun. (2006) 2572.
28. Y. Yu, A. D. Bond, P. W. Leonard, K. P. C. Vollhardt, G. D. Whitener, Angew. Chem. Int. Ed. 45 (2006) 1794.
29. A. Hildebrandt, T. Rüffer, E. Erasmus, J. C. Swarts, H. Lang, Organomet. (2010) 29**.**
30. Z. H. Chohan, M. Praveen, Appl. Organomet. Chem. 15 (2001) 617.
31. K. C. Gupta, A. K. Sutar, Coord. Chem. Rev. 252 (2008) 1420.
32. A. Gul, Z. Akhter, M. Siddiq, S. Sarfraz, B. Mirza. Macrom. 46 (2013) 2800−2807.
33. R. Rajavel, M. S. Vadivu, C. Anitha, Eur. J. Chem. 5 (2008) 620.
34. P. Ghanghas, A. Choudhary, D. Kumar, K. Poonia, Inorg. Chem. Commu. 130, (2021) 108710.
35. A. J. Thomson, H. B. Gray, Curr. Opin. Chem. Biol. (1998) 155–158
36. H. Yu, L, Shao, J. Fang, J. Organomet. Chem. 692 (2007) 991.
37. E. M. Hodnett, J.Med.Chem. 13 (1970) 786.

38. B. Lal, A. Badshah, A. A. Altaf, N. Khan, S. Ullah, Appl. Organomet. Chem. 25 (2011) 843.
39. S. S. Braga, A.M. Silva, Organomet. 32 (2013) 5626.
40. M. F. R. Fouda, M. M. Abd-Elzaher, R. A. Abdelsamaia, Labib. Fouda MFR, Abd-Elzaher MM, Abdelsamaia RA, Labib AA. Appl. Organomet. Chem. 21(2007) 613.
41. V. Kovač, A. Višnjevac, V. Rapić, B. Kojić-Prodić, J. Mol. Stru. 687(2004) 107–110.
42. M. I. Ikhile, J. C. Ngila, Chinese J. Inorg. Chem. 31(2015) 1-10, DOI-10.11862/CJIC.2015.272
43. M. Shabbir, Z. Akhter, I. Ahmad, S. Ahmed, M. Bolte, H. Ismail, B. Mirza, Inorg. Chim Acta. 463 (2017) 102–111.
44. T. J. Sorensen, M. F. Nielsen, Cent. Eur. J. Chem. 9 (2011) 610–618.
45. P. Chaiamornnugool, S. Tontapha, R. Phatchana, Nattawat Ratchapolthavisin, S. Kanokmedhakul, W. Sang-aroon, V. Amornkitbamrung, J. Mol. Struc. 1127 (2017) 145-155.
46. S. Kotteswaran, V. Mohankumar, M. S. Pandian, P. Ramasamy, Inorg. Chim. Acta 467 (2017) 256–263.
47. J. Sivanadanam, R. Mukkamala, S. Mandal, R. Vedarajan, N. Matsumi, I.S. Aidhen, K. Ramanujam, Inter. J. hydro. Energy. (2018) 1-15.
48. M. Abdel-Shakour, W. A. El-Said, I. M. Abdellah, R. Su & A. El-Shafei, J. Mater. Sci: Mater in Electro. 30 (2019) 5081–5091.
49. O. S. Oladeji, M. I. Ikhile, M. Mamo, P. G. Ndungu, D. T. Ndinteh, Chin. J. Inorg Chem. 38 (2022). DOI：10.11862/CJIC.2022.065.
50. P. Mahadevi, S. Sumathi, Synthetic Communi, 50, (2020) 2237-2249.
51. S. Asiri, M. A. Kassem, M. A. Eltaher, K. M, Saad, Int. J. Electrochem. Sci 15, (2020) 6508-6521.
52. S. R. Gupta, P. Mourya, M. M. Singh, V. P. Singh, J. Organ. Chem. 767, (2017) 136-143.

53. S.V. Baryshnikova, A.I. Poddel'sky, A.V. Cherkasov, I.V. Smolyaninov, Inorg Chim Acta, 495, (2019) 118963.

54. E.M. Njogu, B. Omondi, V.O. Nyamori, S. Afr. J. Chem., 69, (2016) 51–66.

55. M. Shabbir, Z Akhter, I. Ahmad, S. Ahmed, M. Bolte, H. Ismail, B. Mirza, Inorgan Chimica Acta 463 (2017) 102–11.